LASER & PHOTONICS REVIEWS
www.lpr-journal.org

Metasurface-Enabled Dual-Channel Single-Pixel Polarimetric Imaging

*Haoran Xiong, Ruizhe Zhao, Chenyi Tian, Xin Li, Bo Wang, Junjie Li, and Lingling Huang**

Single-pixel imaging has garnered significant interest across a variety of research domains due to its cost-effectiveness and adaptability. Metasurfaces, with their subwavelength-scale structures, offer flexible control ability, enabling them to be an ideal platform for single-pixel imaging applications. This study introduces an innovative single-pixel imaging technique that leverages polarization multiplexing metasurfaces to enable dual orthogonal polarization channel imaging from a single measurement. By incorporating four units with varying structural dimensions, 2-bit encoding of the incident light is achieved. Through spatial shifting, images corresponding to different polarization channels with various spatial amplitude masks are encoded independently, resulting in high-quality single-pixel imaging. This multifunctional metasurface streamlines conventional polarization-based single-pixel systems, reducing both time and spatial costs with a single measurement, while achieving a spatial resolution of 4.38 μm in reconstructed images. This innovative approach to polarimetric single-pixel imaging holds great potential for optical detection, target recognition, aviation, and other advanced applications.

1. Introduction

Imaging is a longstanding yet invaluable optical technology that permeates nearly all aspects of daily life, from the advent of pinhole imaging to the development of photography, encompassing industrial manufacturing,[1] medical imaging,[2] and beyond.[3] Imaging is no longer confined to the visible light spectrum[4] but is gradually expanding into broader wavelength bands as research progresses.[5] However, in contrast to the widely used consumer-grade visible Charge coupled Device(CCD) and Complementary Metal Oxide Semiconductor(CMOS) sensors, 2D array sensors in these broader wavelength bands are often prohibitively expensive, posing a significant challenge. Unlike conventional imaging with array sensors, single-pixel imaging requires only a single detector to capture light with spatially encoded information. The object to be measured is under constant illumination with different known masks, and a single pixel detector is used to collect the intensity correspondingly.[6–8] Subsequently, all these masks and intensity information are employed to restore the object information by certain algorithms, including optimization-based algorithms,[9] compressed sensing-based algorithms[10] and deep learning-based algorithms.[11,12] With the ongoing advancement of single-pixel imaging technology, it has progressively found applications across various fields, including terahertz imaging,[13] 3D imaging,[14,15] long-range imaging,[16] ultrafast imaging,[17] polarization imaging,[18–21] and spectral imaging[22–24] and more.[25–27]

Among these, polarization imaging is one of the most essential research areas, with systems classified into four types based on measurement principles: division-of-time, division-of-amplitude, division-of-focal-plane, and division-of-aperture.[28] In the division-of-time, images of different polarization states are captured at different time intervals,[29] while the division-of-amplitude simultaneously captures the amplitude information of all polarization states.[30] Division-of-focal-plane projects different polarization components onto distinct regions of the focal plane,[31] and division-of-aperture allocates polarization information using different polarization elements at the optical system's aperture.[32] Polarization elements play a critical role in these systems, typically combining various polarization components, such as polarizing beam splitters (PBS) or polarizers, to capture information from distinct polarization states. This is achieved either through spatial multiplexing to capture polarization information or by time multiplexing to switch incident polarization states, enabling polarization-sensitive imaging. All these methods rely on multiplex, capturing polarization information either spatially or temporally through multiple detectors or switches. Current single-pixel polarimetric imaging techniques are primarily derived from these systems.[18] By leveraging single-pixel imaging principles, these methods effectively reconstruct images from multiple polarization states. However, they increase the overall system cost and complexity, resulting in a bulky system. There-

H. Xiong, R. Zhao, C. Tian, X. Li, L. Huang
Beijing Engineering Research Center of Mixed Reality and Advanced Display
School of Optics and Photonics
Beijing Institute of Technology
Beijing 100081, China
E-mail: huanglingling@bit.edu.cn

B. Wang, J. Li
Beijing National Laboratory for Condensed Matter Physics
Institute of Physics
Chinese Academy of Sciences
Beijing 100190, China

The ORCID identification number(s) for the author(s) of this article can be found under https://doi.org/10.1002/lpor.202501878

DOI: 10.1002/lpor.202501878

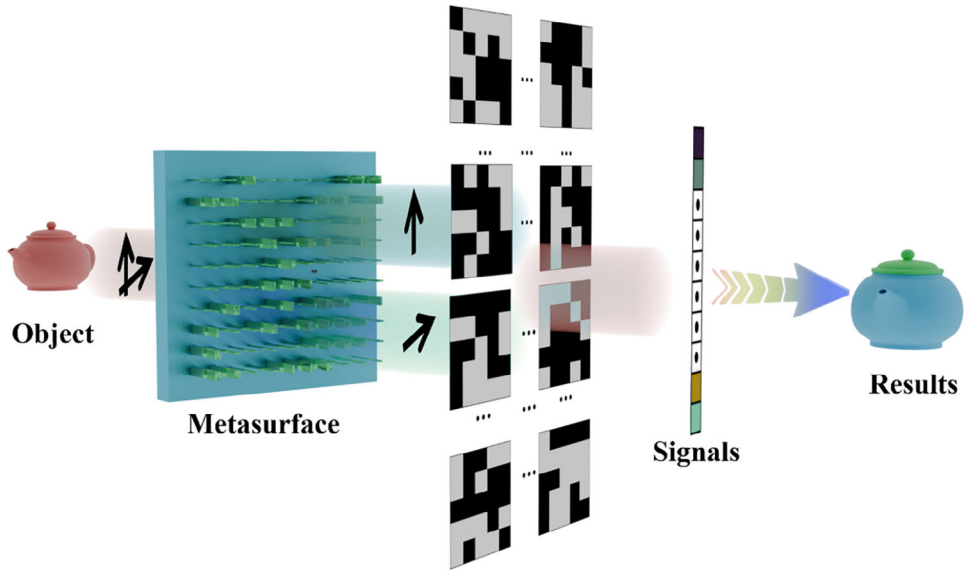

Figure 1. Schematic illustration of the proposed single pixel polarimetric imaging scheme. Light carrying information about an object with unknown polarization is incident on the metasurface, where a series of independent spatial encodings is realized across two orthogonal polarization channels by displacing the metasurface. The corresponding intensity information is then collected by the single pixel detector, allowing for the direct reconstruction of images for both polarization channels using the intensity data and the series of coding masks formed by the metasurface.

fore, there is a pressing need for a simple, multifunctional, and easily integrable device that reduces both spatial and temporal costs, enabling the recovery of multiple polarization states in a single measurement within conventional optical setups.

Currently, the miniaturization and integration of single-pixel imaging systems has become a prevailing trend. Metasurfaces, as ultrathin, man-made 2D arrays with subwavelength unit sizes, can precisely control light at the nanoscale, including amplitude,[33] phase,[34] frequency,[35] polarization,[36] and orbital angular momentum.[37] This is achieved by varying the unit structure size and rotation angles. Metasurfaces are applied in widespread applications, such as holographic displays,[38,39] wavefront manipulation,[40,41] metalenses,[42,43] polarization imaging,[44] and other fields.[45,46] In fact, several schemes are proposed to achieve single-pixel imaging using metasurfaces. In existing schemes, the primary approach is to create a miniature and compact metasurface-based single-pixel imaging system by replacing traditional components, such as the imaging object,[47] modulation mask,[48] or detector,[49] and applying it to high-resolution imaging,[50] multi-color imaging,[49] and information encryption.[51] However, these methods typically consider only a single polarization state for imaging and cannot capture multiple polarization channels, thereby neglecting the inherent polarization-multiplexing capacity of metasurfaces enabled by their anisotropic meta-atoms, which allows simultaneous encoding and retrieval of information across multiple polarization channels in a single measurement.[52–54] Therefore, a metasurface-based single-pixel polarimetric imaging method with intrinsic polarization-multiplexing capability is necessary.

Here, we propose and demonstrate a single-pixel imaging scheme using a polarization multiplexing metasurface. By exploiting the anisotropy of the metasurface unit structure, two independent polarization masks are spatially constructed to achieve 2-bit polarization encoding of the incident light. During imaging, the metasurface is shifted both horizontally and vertically to switch between different spatial masks, enabling modulation and collection of information from both polarization channels with a single detector. The images from different polarization channels can be restored using a modified multi-channel compressed sensing model, achieving a minimum spatial resolution of 4.38 μm and enabling dual-polarization channels imaging in a single measurement. Compared to traditional polarization single-pixel imaging methods, this approach exploits the powerful light-field control capabilities of metasurfaces, eliminating the need for complex and bulky experimental optical paths. This method simplifies the measurement system structure, reduces the time required for multi-channel measurements, lowers imaging costs, and ensures high-quality, high-resolution images. This polarization-based amplitude control scheme enhances the versatility of single-pixel imaging and is expected to offer a novel approach for advanced applications such as industrial inspection, target recognition, and aerospace.

2. Method and Principle

In the single-pixel imaging process, a series of spatial masks and corresponding intensity signals are used in conjunction with specific algorithms to reconstruct the image. As shown in **Figure 1**, light carrying unknown polarization state information from the object is irradiated onto the metasurface, which replaces the commercial digital micromirror device (DMD) and directly serves as a mask to perform binary encodings on the incident light of both polarizations. By selecting metasurface units of different shapes, each unit exhibits different transmittance for x- and y-polarized light, generating two independent random masks on the two channels to achieve polarization encoding of the incident light. When the object's light passes through the metasurface, the intensity information is collected by a single-pixel detector as a

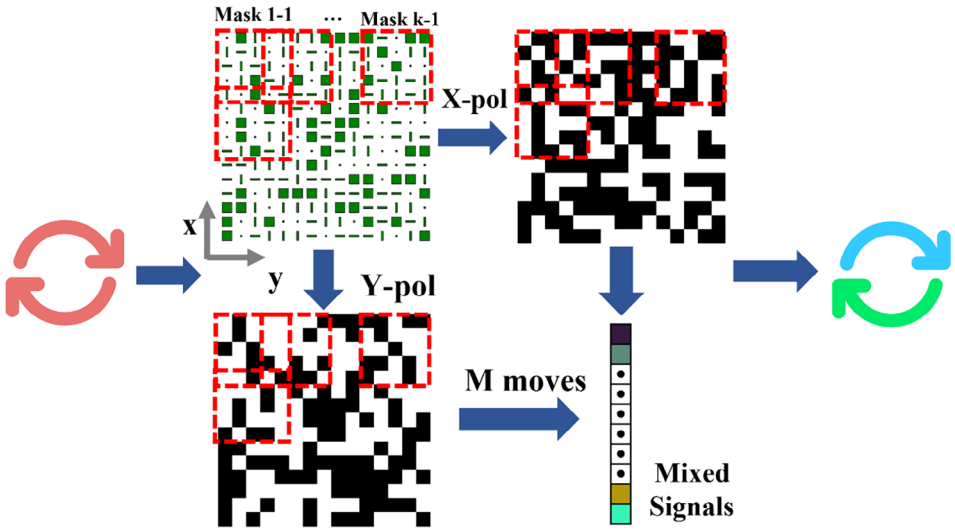

Figure 2. The flow chart of the proposed single pixel polarimetric imaging model. Objects with unknown polarization are projected on metasurfaces that consist of copious polarization-sensitive masks. The masks shown as a red box marked by the dotted line are changed by shifting the metasurface horizontally and vertically. After M moves, the collected mixed signals are used to recover the images in x and y polarization with the SPI algorithm.

detection signal. Finally, by correlating the collected signal with the corresponding metasurface masks, the images of the target object under both x- and y-polarizations are calculated simultaneously using a compressed sensing algorithm with a modified model, based on the total detection intensity and the polarization masks.

Single-pixel imaging technology is particularly suitable for non-visible light bands, with the working wavelength in this study set to 800 nm. Unlike traditional single-pixel imaging methods that use commercial DMDs to provide masks, we employ the amplitude modulation characteristics of metasurfaces to create a spatial binary mask. This characteristic enables similar spatial binary encoding for imaging. However, to obtain polarization information, a single binary encoding method is insufficient. Different amplitude modulations on the x- and y-polarized light are required simultaneously. Therefore, metasurface units capable of varying amplitude responses in different polarization channels are crucial. A significant polarization amplitude modulation difference is determined by two factors: high transmittance under the designed polarization and low transmittance under orthogonal polarization, ensuring a high contrast between the two channels. The metasurface period is set to 500 nm, and the height is 400 nm, with parameter sweeps conducted accordingly. Finally, four structures are selected. These four structures correspond to four distinct functions: transparent to both x- and y-polarizations, highly transparent to x but not y, highly transparent to y but not x, and not transparent to either, forming 2-bit codes (11, 10, 01, 00) for x- and y-polarizations in space. By selecting combinations of these four meta-atoms, any independent binary code for polarization information can be realized in space. The transmission coefficient for parameter sweep and transmission efficiency for selected meta-atoms can be seen in Figures S1 and S2 (Supporting Information).

In single-pixel imaging, spatial information can be encoded using various methods, including random encoding,[55] Hadamard encoding,[56] Fourier encoding,[57] and optimized encoding.[58] Random encoding offers flexibility and noise resistance, making it compatible with the flexible nature of metasurfaces. In our design, random encoding is employed to create two independent masks for the x- and y-polarization channels, with 1 representing transmission and 0 representing non-transmission. For the x- and y-polarization channels, the transmission of each unit is represented by a two-bit combination of 0 and 1, corresponding to distinct unit structures. **Figure 2** illustrates the process of spatial and polarization multiplexing using metasurfaces. The metasurface consists of n × n pixels, with only a subarea of m × m pixels illuminated at a time. By shifting the sample one pixel at a time horizontally and vertically, different masks can be selected sequentially, generating k × k distinct masks, where k = n-m + 1, thus ensuring a large-capacity mask for high-quality imaging. After moving the metasurface M times (where M < k), M intensity values and their corresponding masks can be obtained for subsequent imaging.

Once the single-pixel imaging system is established, the polarization information can be recovered. The polarization state of the light reflected by the object is dependent on the polarization state of the incident light, and the same applies to the transmitted light. The relationship between the incident S_{in} and emitted light S_{out} is described by the following equation:

$$S_{out}(x, y) = M_o(x, y) \cdot S_{in}(x, y) \quad (1)$$

where $S_{in} = [I\ Q\ U\ V]^T$ is the Stokes vector of the incident light, where I is total light intensity, Q is the difference in intensity between the horizontal and vertical polarization components, U is the difference in intensity between the polarization components at +45° and −45° and V is the difference in intensity between the right-handed and left-handed circular polarization components. M_o is the Mueller matrix of the object to be measured.

The general form of the Mueller matrix M_o is:

$$M_O = \begin{pmatrix} m_{00} & m_{01} & m_{02} & m_{03} \\ m_{10} & m_{11} & m_{12} & m_{13} \\ m_{20} & m_{21} & m_{22} & m_{23} \\ m_{30} & m_{31} & m_{32} & m_{33} \end{pmatrix} \tag{2}$$

which is a 4 × 4 real matrix widely used in optics, providing a complete description of an optical system and transforming the polarization state of light. Each matrix element corresponds to specific polarization interactions: the m_{nn} term represents total intensity transmission, while m_{n1} and m_{1n} quantify horizontal linear diattenuation effects, with m_{02} and m_{20} capturing ±45° linear diattenuation. Circular diattenuation manifests in m_{03} and m_{30} components, whereas linear retardance is encoded in the m_{11}, m_{12}, m_{21}, and m_{22} elements. Circular retardance emerges through m_{13}, m_{31}, m_{23}, and m_{32} terms, and the m_{33} element reflects depolarization strength. Collectively, these 16 parameters enable comprehensive quantification of material optical anisotropies, including dichroic absorption, birefringence, chiral responses, and polarization scrambling phenomena.[59]

Similarly, for our designed metasurface, which can function as dual-polarizers, it can be represented by a corresponding Mueller matrix:

$$M_{ms}(x,y) = \frac{1}{2}B_1(x,y)\cdot\begin{pmatrix} 1 & 1 & 0 & 0 \\ 1 & 1 & 0 & 0 \\ 0 & 0 & 0 & 0 \\ 0 & 0 & 0 & 0 \end{pmatrix} + \frac{1}{2}B_2(x,y)\cdot\begin{pmatrix} 1 & -1 & 0 & 0 \\ -1 & 1 & 0 & 0 \\ 0 & 0 & 0 & 0 \\ 0 & 0 & 0 & 0 \end{pmatrix}$$

$$= \begin{pmatrix} \frac{1}{2}(B_1(x,y)+B_2(x,y)) & \frac{1}{2}(B_1(x,y)-B_2(x,y)) & 0 & 0 \\ \frac{1}{2}(B_1(x,y)-B_2(x,y)) & \frac{1}{2}(B_1(x,y)+B_2(x,y)) & 0 & 0 \\ 0 & 0 & 0 & 0 \\ 0 & 0 & 0 & 0 \end{pmatrix} \tag{3}$$

where $B_1(x,y)$ and $B_2(x,y)$ correspond to random binary masks under the x and y polarization channels, respectively. Since each channel exclusively encodes a single polarization state, this configuration effectively emulates the action of a linear polarizer aligned along the corresponding polarization axis. The resultant modulation is derived from the coherent superposition of contributions from both orthogonal polarization channels.

Therefore, for a single signal acquisition, Equation (1) can be rewritten as:

$$S_{out,i}(x,y) = M_{ms,i}(x,y)\cdot M_o(x,y)\cdot S_{in}(x,y) \tag{4}$$

When the incident light polarization is fixed to be x-polarized, we obtain:

$$S_{out,i}(x,y) = \begin{pmatrix} \frac{1}{2}(m_{00}+m_{01}+m_{10}+m_{11})B_{1,i}(x,y) \\ +\frac{1}{2}(m_{00}+m_{01}-m_{10}-m_{11})B_{2,i}(x,y) \\ \frac{1}{2}(m_{00}+m_{01}+m_{10}+m_{11})B_{1,i}(x,y) \\ +\frac{1}{2}(m_{10}+m_{11}-m_{00}-m_{01})B_{2,i}(x,y) \\ 0 \\ 0 \end{pmatrix} \tag{5}$$

Since only one intensity value can be detected, we ultimately obtain an intensity value I_{out} that contains information in both the x and y polarization channels from the object.

$$I_{out,i}(x,y) = \frac{1}{2}(m_{00}+m_{01}+m_{10}+m_{11})B_{1,i}(x,y) + \frac{1}{2}(m_{00}+m_{01}-m_{10}-m_{11})B_{2,i}(x,y) \tag{6}$$

By applying Stokes parameter analysis to the polarization-multiplexed signal, I_{out} represents the summation of the products between the polarization masks and the corresponding polarization information. Meanwhile, the acquisition of multiplexed intensity signals containing dual-polarization channel information necessitates a robust framework for polarization-resolved target reconstruction. In this work, we advance conventional single-pixel imaging methodologies by formulating a dual-channel polarization-decoupled reconstruction framework based on compressed sensing. The proposed model addresses the challenge of reconstructing polarization-multiplexed intensity signals by reformulating the mixed encoding process into a unified matrix representation. Crucially, the proposed formulation transforms the mixed-signal inverse problem into a standard single-pixel imaging architecture, thereby enabling efficient reconstruction through established sparse recovery algorithms. A comprehensive derivation of the framework and its numerical validation are provided in Section S2 (Supporting Information).

For image reconstruction, we employ the Two-Step Iterative Shrinkage/Thresholding (TwIST) algorithm,[60] a compressed sensing-based optimization framework widely adopted in single-pixel imaging to recover high-fidelity images from underdetermined measurements. Based on the principles of compressed sensing, TwIST iteratively minimizes reconstruction errors while enforcing image sparsity through a two-step procedure. The algorithm alternates between these steps to iteratively update the signal estimate: initially, the Iterative Shrinkage Thresholding (ISTA) method is applied to reduce the reconstruction error; subsequently, a two-step iterative strategy is employed to further refine the estimate, effectively converging toward the optimal solution. This approach significantly reduces computational complexity while preserving the integrity and quality of the reconstructed image.

In essence, this method utilizes two independent amplitude-modulated masks to spatially encode the x- and y-polarized light

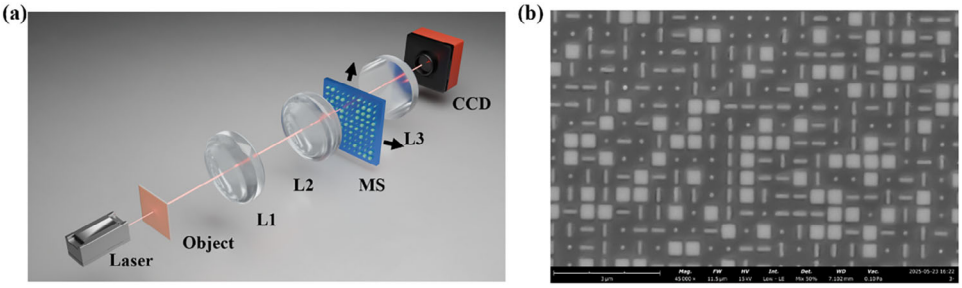

Figure 3. a) Experimental setup schematic. A laser source illuminates the imaging object. Lenses L_1 and L_2 demagnify and project the object onto the polarization-dependent modulation masks. The dual arrows indicate a translation stage that spatially shifts the metasurface to switch between masks. Lens L_3 focuses the modulated light onto a CCD camera, functioning as a single-pixel detector. b) Scanning electron microscopy (SEM) images confirming the successful fabrication of all four designed meta-atom types.

components. Through a zigzag scanning pattern implemented by the metasurface, the polarization-resolved spatial information of the target is multiplexed into a single composite intensity signal. The metasurface's compact multiplexed design facilitates seamless integration of dual polarization channels within a single unified optical system. At the detection stage, the polarization-multiplexed signal is captured by a single-pixel detector and reconstructed via a newly proposed polarimetric imaging model—a computational framework that decouples the mixed signal by leveraging sparsity constraints and polarization orthogonality. This approach achieves high-fidelity recovery of both polarization-resolved target images while maintaining minimal hardware complexity.

3. Results

Building upon the design and algorithm outlined above, we conducted simulations and completed the experiment.

Initially, we assess the impact of the mixed signal recovery model on the compressed sensing algorithm by comparing the quality of restored images at various compression ratios. In the simulation, the letters "R" and "F", each measuring 100 × 100 pixels, are chosen to represent the information of the x and y channels respectively, and input together as a mixed signal. These two letters lack rotational symmetry, enhancing the generalizability of the results. Afterward, light containing mixed information is directed onto the corresponding area of the metasurface, it is randomly encoded in two channels, and the intensity value is subsequently collected on the focal plane. A series of intensity values is linked to the mask and restored using the previously described polarization single-pixel imaging model. Additionally, Structural Similarity Index Measure (SSIM) and Peak Signal-to-Noise Ratio (PSNR) metrics are used to evaluate image quality. We also compare the SSIM and PSNR values for single-channel restoration, using the letter "R" for the single-channel image. The mixed signal recovery model affects the minimum compression rate required to achieve acceptable results, due to the inclusion of more target objects. However, this influence does not affect the stability of the multi-channel restoration model. When the compression rate exceeds 30%, satisfactory results are achieved, demonstrating that our restoration model is effective for multi-channel complex image restoration. Therefore, 30% is set to be the compression rate in the further experiment. The simulation results at different sampling ratios with the proposed modified single pixel imaging model are shown in Figure S3 (Supporting Information).

Next, we perform the experiment. The experimental optical setup is illustrated in **Figure 3**a. After passing through the target object, the light is imaged onto the metasurface via a set of lenses with a minification ratio, and is modulated by a series of randomly coded masks. The light is then focused by the lens and captured by the detector. The metasurface has a resolution of 1000 × 1000 pixels, with a period of 500 nm. Figure 3b presents a scanning electron microscope image of the metasurface, revealing that the fabricated nanostructures exhibit a high degree of conformity with the design specifications, demonstrating excellent agreement between design and fabrication. By shifting the metasurface in x and y directions and altering the coding masks with a moving platform, different intensity values can be obtained, placing high demands on alignment and movement precision.

To thoroughly evaluate the imaging performance of the device, we first test a polarization-independent object, set the sampling rate to 30% and use the letter "G" as the target image, which is loaded onto the DMD. A set of lenses is employed to match the image size with that of the metasurface mask. Before placing the sample, we capture its image using the CCD. Subsequently, the sample is positioned at the back focal plane of the front lens group. For detection, a lens and CCD combination is used in place of a single-pixel detector to collect the encoded intensity. The recovery results for both channels are shown in **Figure** 4a. The polarization images are shown in pseudo-color images to represent different polarizations.

Next, we test polarization-dependent objects. In this experiment, we use a combination of linear polarizers to characterize the polarization states across different regions. Specifically, we select two curved arrows, positioned vertically, with the upper and lower sections representing x and y polarizations, respectively. Similarly, we first capture images under different polarization channels by placing a polarizer in front of the CCD. We then remove the polarizer, directly detect the mixed intensity information, and restore it using the compressed sensing algorithm. The captured and restored results are shown in Figure 4b. Meanwhile, the pseudo-color images of both objects are generated from the results in the two polarization channels, providing a clearer depiction of the polarization distribution.

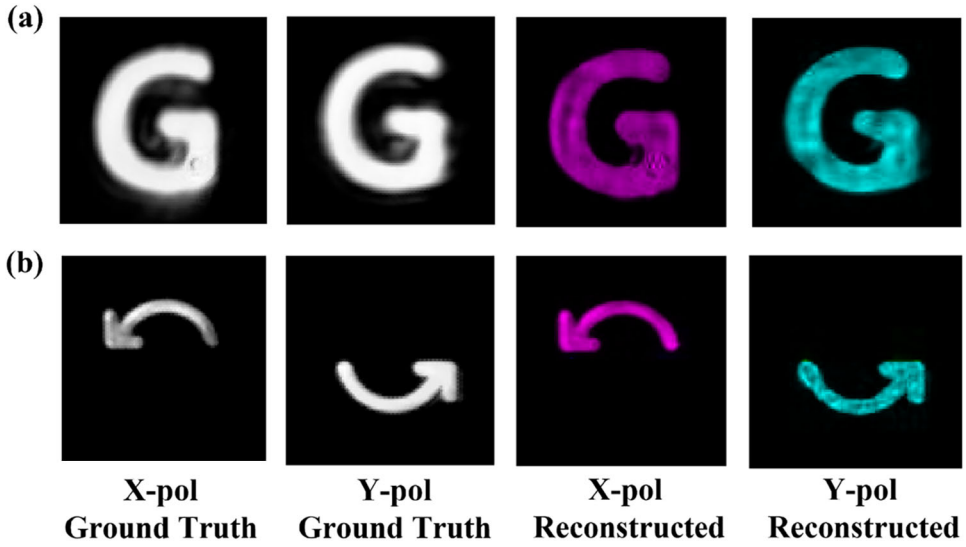

Figure 4. Experimental results for polarization-independent and polarization-dependent objects. a) The letter "G" is selected as the target, with reconstructed images shown under both x-polarization and y-polarization. The pseudo-color images are used to indicate different polarizations. b) An image consisting of an upper curved arrow and a lower curved arrow, representing x-polarization and y-polarization, respectively.

Finally, an object is used to further illustrate the ability of this method to image a metasurface sample designed to generate a vector vortex beam with topological charge $p = 6$. The microscopic image of the sample is shown in **Figure** 5a. The polarization restoration results, captured by a CCD camera and processed using our model, are presented in Figure 5b. These results closely align with the expected outcomes, demonstrating the accuracy of the model. The detailed optical setups for different objects are shown in Figure S4 (Supporting Information).

By fusing the two reconstructed polarization states, we generate a polarization pseudo-color image in Figure 5c to visualize spatially varying polarization responses. Further quantitative analysis is performed through the derived polarization contrast (PC) $PC = \frac{|I_x - I_y|}{I_x + I_y}$ and ellipticity maps $\xi = \tan^{-1}(\sqrt{\frac{I_x}{I_y}})$ in Figure 5d, which collectively reveal the metasurface-induced single pixel polarimetric imaging characteristics.

These results systematically validate the scheme's capability to decode polarimetric information via single-pixel detection. The synergy between the metasurface's spatially tailored polarization manipulation and the computational imaging model enables simultaneous recovery of dual-polarization channels, overcoming the conventional single-pixel systems limitation in polarization dimensionality without resorting to bulky polarization optics. This advancement paves the way for deployable polarimetric imaging in resource-constrained scenarios, where rapid characterization of polarization contrast and ellipticity is critical.

To quantitatively assess the imaging performance, we employ the USAF1951 resolution target as a benchmark. Experimental results demonstrate distinguishable 1D horizontal lines in Group 6, where Group 6 refers to a resolution tier in the USAF 1951 test chart, and its finest pattern (Element 6) corresponds to 114 line pairs per millimeter (Section S4, Supporting Information). Resolving these lines demonstrates a minimum feature size of 4.38 μm in our system while maintaining polarimetric sensitivity. The experimental results for the resolution target and the corresponding test chart are shown in Figure S5 and Table S1 (Supporting Information)

The proposed single-pixel polarimetric imaging scheme achieves high-resolution polarization imaging by integrating a metasurface-enabled computational model with compressed sensing. Dual-polarization channel reconstruction demonstrates successful recovery of polarization information at a 30% compression rate while maintaining high spatial resolution. This performance overcomes the long-standing trade-off between polarization-information richness and system practicality in single-pixel architectures, enabling parallel acquisition of spatial details and polarization signatures without multi-detector arrays, a critical advancement beyond conventional sequential polarization measurement paradigms.

4. Discussion and Conclusion

In this work, we propose a single-pixel imaging scheme based on polarization multiplexing metasurfaces. By integrating an improved polarization single-pixel imaging model with a compressed sensing algorithm, our method enables the simultaneous restoration of images from two polarization channels through a single-pixel process. We design four distinct metasurface units based on polarization response characteristics, creating a 2-bit spatial light encoding for x and y polarizations. This allows for independent amplitude encoding of the incident light using a single metasurface.

During the single-pixel imaging process, the metasurface forms a series of independent binary masks in space. These masks are crucial for achieving high-quality imaging. The collected intensity values are then input into the modified polarization single-pixel model, enabling the restoration of both polarization images simultaneously. This approach takes advantage of the flexible control capabilities of the metasurface, eliminating the need for additional detectors. By combining polarization-based amplitude control with an effective recovery algorithm, we sig-

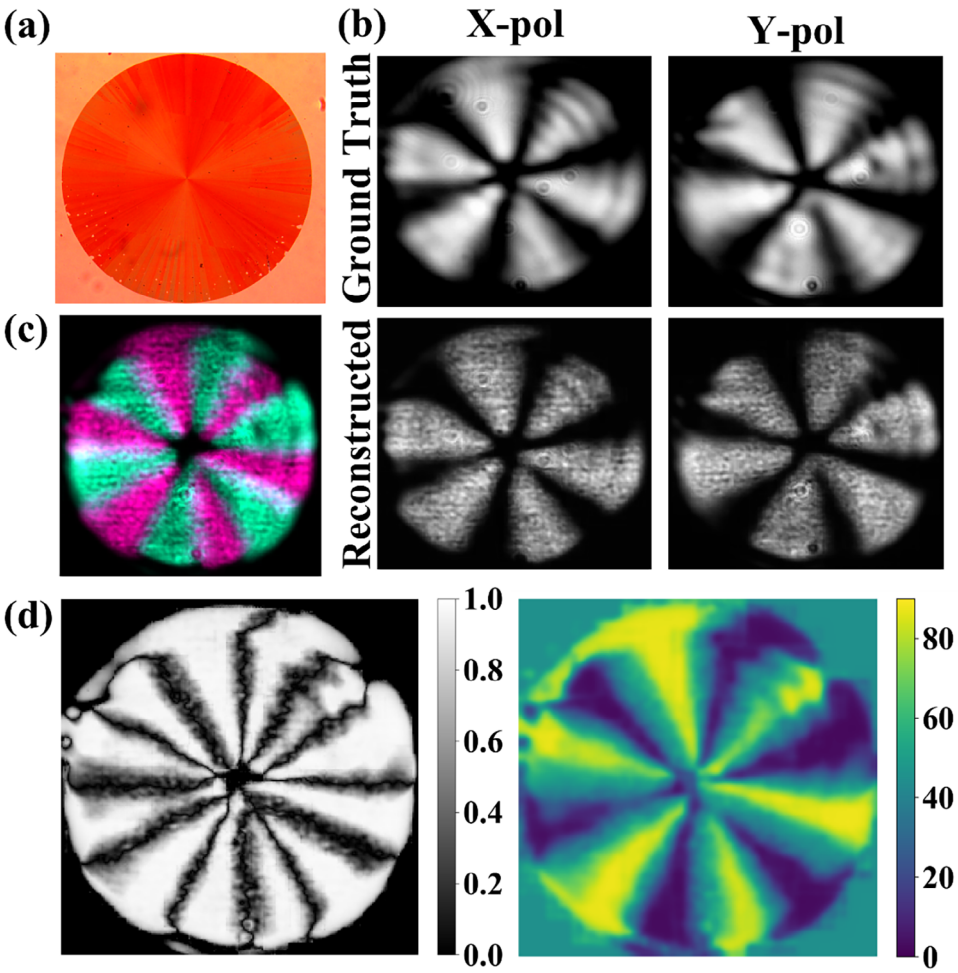

Figure 5. Experimental results for a real object. a) The microscopic image for the metasurface sample. b) The ground truth and the reconstructed images for the sample. c) The reconstructed pseudo color image based on two linear polarized channels. d) The Polarization Contrast and Ellipticity for the retrieved results. PC measures polarization anisotropy, ranging from 0 (isotropic) to 1 (fully polarized). ξ indicates the angle of the dominant polarization component.

nificantly reduce the impact of polarization on the system's complexity. Furthermore, such a metasurface minimizes the data and time requirements associated with multi-channel imaging. Overall, this method offers an efficient and cost-effective polarization single-pixel imaging solution with potential applications in computer vision, environmental monitoring, medical imaging, etc.

The metasurface's design flexibility establishes a scalable platform for advancing polarimetric imaging beyond dual-polarization capabilities. By engineering metasurface units with enhanced polarization selectivity, such as incorporating highly anisotropic meta-atoms exhibiting strong dichroic responses, the encoding channels can be multiplicatively expanded to resolve complex polarization states (e.g., full Stokes parameters). This progression from binary to multi-bit polarization encoding enables high-dimensional polarimetric reconstruction, while algorithm-hardware co-design strategies could further minimize sampling overhead. Crucially, such scalability transcends mere channel count increases and embodies a paradigm shift toward multivariate single-pixel sensing. This approach unlocks applications in scenarios requiring concurrent spatial and polarization resolution, including optical detection, target recognition, aviation, and other advanced applications.

Supporting Information

Supporting Information is available from the Wiley Online Library or from the author.

Acknowledgements

The authors acknowledge funding provided by the National Natural Science Foundation of China program (No. U21A20140), the National Key R&D Program of China (2021YFA1401200), and the Beijing Natural Science Foundation (JQ24028). This work was supported by the Synergetic Extreme Condition User Facility (SECUF).

Conflict of Interest

The authors declare no conflict of interest

Author Contributions

H.X. and L.H. proposed the idea. H.X. conducted pattern designs and numerical simulations. B.W. and J.L. fabricated the samples. H.X. performed the measurements. H.X. and L.H. prepared the manuscript. L.H. supervised the overall projects. All the authors analyzed the data and discussed the results.

Data Availability Statement

The data that support the findings of this study are available from the corresponding author upon reasonable request.

Keywords

compressed sensing, dielectric metasurfaces, polarimetric imaging, single-pixel imaging

Received: July 17, 2025
Revised: August 28, 2025
Published online:

[1] Y. Shimizu, L.-C. Chen, D. W. Kim, X. Chen, X. Li, H. Matsukuma, *Meas. Sci. Technol.* **2021**, *32*, 042003.
[2] B. Shen, C. Luo, W. Pang, Y. Jiang, W. Wu, R. Hu, J. Qu, B. Gu, L. Liu, *PhotoniX* **2024**, *5*, 1.
[3] C. Rogers, A. Y. Piggott, D. J. Thomson, R. F. Wiser, I. E. Opris, S. A. Fortune, A. J. Compston, A. Gondarenko, F. Meng, X. Chen, G. T. Reed, R. Nicolaescu, *Nature* **2021**, *590*, 256.
[4] X. Hua, Y. Wang, S. Wang, X. Zou, Y. Zhou, L. Li, F. Yan, X. Cao, S. Xiao, D. P. Tsai, J. Han, Z. Wang, S. Zhu, *Nat. Commun.* **2022**, *13*, 2732.
[5] H. He, Y. Zhang, Y. Shao, Y. Zhang, G. Geng, J. Li, X. Li, Y. Wang, L. Bian, J. Zhang, L. Huang, *Adv. Mater.* **2024**, *36*, 2313357.
[6] M. P. Edgar, G. M. Gibson, M. J. Padgett, *Nature Photon* **2019**, *13*, 13.
[7] G. M. Gibson, S. D. Johnson, M. J. Padgett, *Opt. Express* **2020**, *28*, 28190.
[8] L. Martínez-León, P. Clemente, Y. Mori, V. Climent, J. Lancis, E. Tajahuerce, *Opt. Express* **2017**, *25*, 4975.
[9] L. Bian, J. Suo, Q. Dai, F. Chen, *J. Opt. Soc. Am. A* **2018**, *35*, 78.
[10] O. Katz, Y. Bromberg, Y. Silberberg, *Appl. Phys. Lett.* **2009**, *95*, 131110.
[11] F. Wang, C. Wang, C. Deng, S. Han, G. Situ, *Photon. Res.* **2022**, *10*, 104.
[12] Z. Yang, Y. u.-M. Bai, L. i.-D. a. Sun, K. e.-X. Huang, J. Liu, D. Ruan, J.-L. Li, *Photonics* **2021**, *8*, 400.
[13] R. I. Stantchev, B. Sun, S. M. Hornett, P. A. Hobson, G. M. Gibson, M. J. Padgett, E. Hendry, *Sci. Adv.* **2016**, *2*, 1600190.
[14] B. Sun, M. P. Edgar, R. Bowman, L. E. Vittert, S. Welsh, A. Bowman, M. J. Padgett, *Science* **2013**, *340*, 844.
[15] Y. Zhang, M. P. Edgar, B. Sun, N. Radwell, G. M. Gibson, M. J. Padgett, *J. Opt.* **2016**, *18*, 035203.
[16] W. Gong, C. Zhao, H. Yu, M. Chen, W. Xu, S. Han, *Sci. Rep.* **2016**, *6*, 26133.
[17] Z.-H. Xu, W. Chen, J. Penuelas, M. Padgett, M.-J. Sun, *Opt. Express* **2018**, *26*, 2427.
[18] V. Durán, P. Clemente, M. Fernández-Alonso, E. Tajahuerce, J. Lancis, *Opt. Lett.* **2012**, *37*, 824.
[19] S. S. Welsh, M. P. Edgar, R. Bowman, B. Sun, M. J. Padgett, *J. Opt.* **2015**, *17*, 025705.
[20] A. S. Chirkin, P. P. Gostev, D. P. Agapov, S. A. Magnitskiy, *Laser Phys. Lett.* **2018**, *15*, 115404.
[21] S. Dongfeng, Z. Jiamin, H. Jian, W. Yingjian, Y. Kee, C. Kaifa, X. Chenbo, L. Dong, Z. Wenyue, *Optic. Lasers in Eng.* **2018**, *102*, 100.
[22] Z. Zhang, S. Liu, J. Peng, M. Yao, G. Zheng, J. Zhong, *Optica* **2018**, *5*, 315.
[23] F. Soldevila, E. Irles, V. Durán, P. Clemente, M. Fernández-Alonso, E. Tajahuerce, J. Lancis, *Appl. Phys. B* **2013**, *113*, 551.
[24] S. S. Welsh, M. P. Edgar, R. Bowman, P. Jonathan, B. Sun, M. J. Padgett, *Opt. Express* **2013**, *21*, 23068.
[25] H. Takatsuka, M. Yasugi, S. Suyama, H. Yamamoto, *Optical Review* **2024**, *31*, 116.
[26] B. Lochocki, A. Gambín, S. Manzanera, E. Irles, E. Tajahuerce, J. Lancis, P. Artal, *Optica, OPTICA* **2016**, *3*, 1056.
[27] S. Ota, R. Horisaki, Y. Kawamura, M. Ugawa, I. Sato, K. Hashimoto, R. Kamesawa, K. Setoyama, S. Yamaguchi, K. Fujiu, K. Waki, H. Noji, *Science* **2018**, *360*, 1246.
[28] J. S. Tyo, D. L. Goldstein, D. B. Chenault, J. A. Shaw, *Appl. Opt.* **2006**, *45*, 5453.
[29] L. Bigué, N. Cheney, *Polarization Science and Remote Sensing III* **2007**, *6682*, 668205.
[30] A. M. El-Saba, R. M. A. Azzam, M. a. G. Abushagur, *Opt. Lett.* **1996**, *21*, 1709.
[31] S. B. Powell, V. Gruev, *Opt. Express* **2013**, *21*, 21039.
[32] J. L. Pezzaniti, D. B. Chenault, *Polarization Science and Remote Sensing II* **2005**, *5888*, 239.
[33] A. C. Overvig, S. Shrestha, S. C. Malek, M. Lu, A. Stein, C. Zheng, N. Yu, *Light: Science & Applications* **2019**, *8*, 92.
[34] N. Yilmaz, A. Ozer, A. Ozdemir, H. Kurt, *J. Phys. D: Appl. Phys.* **2019**, *52*, 205102.
[35] Y. Yin, Q. Jiang, H. Wang, J. Liu, Y. Xie, Q. Wang, Y. Wang, L. Huang, *Adv. Mater.* **2024**, *36*, 2312303.
[36] J. P. B. Mueller, N. A. Rubin, R. C. Devlin, B. Groever, F. Capasso, *Phys. Rev. Lett.* **2017**, *118*, 113901.
[37] J. Chu, D. Chu, Q. Smithwick, *Research* **2019**, *2019*, 1.
[38] J. Ko, G. Kim, I. Kim, S. H. Hwang, S. Jeon, J. Ahn, Y. Jeong, J.-H. Ha, H. Heo, J.-H. Jeong, I. Park, J. Rho, *Advanced Science* **2024**, *11*, 2407045.
[39] R. Zhao, B. Sain, Q. Wei, C. Tang, X. Li, T. Weiss, L. Huang, Y. Wang, T. Zentgraf, *Light: Science & Applications* **2018**, *7*, 95.
[40] X. Li, X. Li, X. Zhang, R. Zhao, G. Geng, J. Li, L. Huang, Y. Wang, *Laser Photonics Rev.* **2022**, *17*, 2100592.
[41] X. Zhang, X. Li, H. Zhou, Q. Wei, G. Geng, J. Li, X. Li, Y. Wang, L. Huang, *Adv. Funct. Mater.* **2022**, *32*, 2209460.
[42] Q. Jiang, J. Liu, J. Li, X. Jing, X. Li, L. Huang, Y. Wang, *Adv. Opt. Mater.* **2023**, *11*, 2300077.
[43] Y. Li, S. Chen, H. Liang, X. Ren, L. Luo, Y. Ling, S. Liu, Y. Su, S.-T. Wu, *PhotoniX* **2022**, *3*, 29.
[44] Y. Zhang, M. Pu, J. Jin, X. Lu, Y. Guo, J. Cai, F. Zhang, Y. Ha, Q. He, M. Xu, X. Li, X. Ma, X. Luo, *Opto-Electron. Adv.* **2022**, *5*, 11.
[45] L. Zhang, H. Zhan, X. Liu, H. Cao, F. Xing, Z. You, *PhotoniX* **2024**, *5*, 21.
[46] R. Zhao, L. Huang, Y. Wang, *PhotoniX* **2020**, *1*, 20.
[47] H.-C. Liu, B. Yang, Q. Guo, J. Shi, C. Guan, G. Zheng, H. Mühlenbernd, G. Li, T. Zentgraf, S. Zhang, *Sci. Adv.* **2017**, *3*, 1701477.
[48] J. Yan, Y. Wang, Y. Liu, Q. Wei, X. Zhang, X. Li, L. Huang, *Nanophotonics* **2022**, *11*, 3071.
[49] J. Xiong, Z.-H. Zhang, Z. Li, P. Zheng, J. Li, X. Zhang, Z. Gao, Z. Wei, G. Zheng, S.-P. Wang, H.-C. Liu, *Light Sci Appl* **2023**, *12*, 286.
[50] W. Li, J. Qi, A. Alu, *Photon. Res.* **2024**, *12*, 2311.
[51] P. Zheng, Q. Dai, Z. Li, Z. Ye, J. Xiong, H.-C. Liu, G. Zheng, S. Zhang, *Sci. Adv.* **2021**, *7*, abg0363.
[52] A. Zaidi, N. A. Rubin, M. L. Meretska, L. W. Li, A. H. Dorrah, J.-S. Park, F. Capasso, *Nat. Photon.* **2024**, *18*, 704.

[53] L. W. Li, J. Oh, H. Miller, F. Capasso, N. A. F. Rubin, *Optica* **2025**, *12*, 799.
[54] R. Zhao, Q. Wei, Y. Li, X. Li, G. Geng, X. Li, J. Li, Y. Wang, L. Huang, *Laser Photonics Rev.* **2023**, *17*, 2200982.
[55] S. Jiao, J. Feng, Y. Gao, T. Lei, X. Yuan, *Opt. Express* **2020**, *28*, 7301.
[56] E. Hahamovich, S. Monin, Y. Hazan, A. Rosenthal, *Nat. Commun.* **2021**, *12*, 4516.
[57] Z. Zhang, X. Ma, J. Zhong, *Nat. Commun.* **2015**, *6*, 6225.
[58] C. F. Higham, R. Murray-Smith, M. J. Padgett, M. P. Edgar, *Sci. Rep.* **2018**, *8*, 2369.
[59] C. He, H. He, J. Chang, B. Chen, H. Ma, M. J. Booth, *Light Sci Appl* **2021**, *10*, 194.
[60] J. M. Bioucas-Dias, M. A. T. Figueiredo, *IEEE Transact. Image Process.* **2007**, *16*, 2992.